LAWRENCE
LIVERMORE
NATIONAL
LABORATORY

UCRL-JRNL-227913

K-alpha conversion efficiency measurments for x-ray scattering in inertial confinement fusion plasmas

A. L. Kritcher, P. Neumayer, M. K. Urry, H. Robey, C. Niemann, O. L. Landen, E. Morse, S. H. Glenzer

February 11, 2007

High Energy Density Physics

K-alpha conversion efficiency measurements for x-ray scattering in inertial confinement fusion plasmas

A. L. Kritcher*†, P. Neumayer*, M. K. Urry*, H. Robey*, C. Niemann‡, O.L.Landen*, E. Morse†, and S. H. Glenzer*
*L-399, Lawrence Livermore National Laboratory,
University of California, P.O. Box 808, Livermore, CA 94551, USA
† Nuclear Engineering Department, University of California Berkeley, Berkeley, CA 94709 and
‡Electrical Engineering Department, University of California Los Angeles,
Box 951594, Los Angeles, CA 90095-1594, USA
(Dated: December 11, 2006)

The conversion efficiency of ultra short-pulse laser radiation to K-α x-rays has been measured for various chlorine-containing targets to be used as x-ray scattering probes of dense plasmas. The spectral and temporal properties of these sources will allow spectrally-resolved x-ray scattering probing with picosecond temporal resolution required for measuring the plasma conditions in inertial confinement fusion experiments. Simulations of x-ray scattering spectra from these plasmas show that fuel capsule density, capsule ablator density, and shock timing information may be inferred.

PACS numbers: 52.25.Os, 52.35.Fp, 52.50.Jm
Keywords: X-ray spectra, Conversion efficiency, Compton scattering, dense Plasmas

INTRODUCTION

Recent demonstration of spectrally resolved x-ray scattering for measuring temperatures and densities in solid-density plasmas has enabled new applications, e.g., measurements of the equation of state, phase transitions, and the compressibility of dense matter [1–3]. In the first experiments, energetic nanosecond lasers have been employed for illuminating foil targets producing spectrally narrow K lines in highly ionized helium-like or hydrogen-like atoms. These x-ray lines have been subsequently scattered in single-shot experiments from solid density plasmas and detected by highly efficient Bragg crystals [4, 5]. High conversion efficiencies together with the narrow bandwidth provided sufficient photon numbers at the K-line energy allowing spectrally-resolved measurements from dynamically heated solids. Experiments in backscattering and forward scattering geometry have successfully observed the Compton downshifted line [2] and plasmon line [1], respectively, providing accurate information of the plasma conditions. A temporal resolution of the measured spectra, approximately 100 ps, has been obtained by gated microchannelplate detectors sufficient for measuring the conditions in radiatively heated matter.

For the characterization of strong shocks in dense matter, however, it will be advantageous to develop x-ray sources that provide picosecond temporal resolution over a small scattering volume. Laser-driven shock features may spatially extend over a region smaller than 10μm and pass through 10μm of solid density matter within less than 100ps. Thus, x-ray sources with < 10 ps duration [**?**] will virtually provide a snap shot of the shock features while traversing through a 10μm long scattering volume that can be defined with collimating slits [7] in a scattering experiment.

At present, ultra-short pulse laser-produced K$-\alpha$ radiation [8–10], free electron lasers [11–14], and soft x-ray lasers [15, 16] are investigated to provide the required short x-ray pulses for scattering measurements. However, the simultaneous stringent requirements on brightness, bandwidth, and x-ray energy indicate that the first x-ray scattering experiments with high temporal resolution of < 10 ps may be attempted with K$-\alpha$ radiation. This source has the additional advantage of being available together with long-pulse lasers [17] to drive shocks in planar geometry and in spherical geometry in inertial confinement fusion capsule implosions on the National Ignition Facility [19] .

In this study, we have measured ultra-short pulse laser produced K$-\alpha$ radiation of chlorine-containing targets demonstrating conversion efficiencies, ratio of laser energy conversion to K-$-\alpha$ production, of 2×10^{-5}. Only weak dependencies on target thickness and material have been observed, thus limiting the present number of K$-\alpha$ photons available for scattering experiments to be 2 orders of magnitude smaller than for long-pulse laser produced K-lines at comparable laser energies [10, 20]. Thus, to increase the number of detected photons in a K$-\alpha$ scattering experiment, improved detection techniques, such as developing higher efficiency crystals [10], must be adopted. On the other hand, the x-ray spectra show that the small bandwidth of $\Delta E/E = 2 \times 10^{-3}$ and the complete lack of satellites on the red wing of the K$-\alpha$ line provide optimum spectral properties for resolving the Compton and plasmon features in the x-ray scattering spectrum. In particular, the latter is only shifted from the incident x-ray energy by < 50 eV, which can be resolved by the K$-\alpha$ radiation.

The present experiments have studied K$-\alpha$ production and spectra at moderate x-ray energies. This choice is motivated by the fact that hard x rays with energies

much above 10 keV may only be used for non-collective regime applications in dynamically heated experiments. Moderate x-ray energies, on the other hand, will allow both Compton and plasmon measurements as long as plasma densities are not extreme and the x-rays effectively penetrate through the plasma.

In Section II we will describe x-ray scattering regimes and features in the K-α scattering spectrum that will allow us to extract diagnostic information. In Section III we will present K$-\alpha$ source measurements and the calibration of the detectors. Section IV presents calculations of K$-\alpha$ scattering spectra to characterize inertial confinement fusion capsule implosion conditions and Section V will present the conclusions.

X-RAY SCATTERING IN DENSE PLASMAS

Spectrally resolved x-ray scattering measurements have been first applied in warm solid-density plasmas in the non-collective regime using a titanium He$-\alpha$ source. Important plasma parameters, including electron temperature and density, were extracted from the scattered spectra. More recently, novel measurement techniques have become important to determine the optical properties of dense plasmas by probing the frequency response of plasma oscillations. Therefore, a low energy 2.62 keV Cl K-α x-ray probe has been developed.

Collective scattering probes plasma scale lengths larger than the plasma screening length, λ_S, which can be approximated by the Thomas-Fermi length for a degenerate system. The Thomas-Fermi screening length, λ_{TF}, is given by $1/k_{TF}$ where

$$k_{TF}^2 = \frac{6\pi n_e e^2}{\epsilon_F} \tag{1}$$

$$\epsilon_F = \frac{\hbar^2 \left(3\pi^2 n_e\right)^{2/3}}{2m_e}$$

where n_e is the electron density, and ϵ_F is the Fermi energy of the system. This yields the Thomas-Fermi screening length

$$\lambda_{TF} = \sqrt{\frac{\hbar^2}{4m_e e^2}\left(\frac{\pi}{3n_e}\right)^{1/3}} \tag{2}$$

with m_e being the mass of the electron, e the electric charge, and $h = 2\pi\hbar$ is Planck's constant. For a classical plasma, λ_S is given by the Debye length,

$$\lambda_D = \left(\epsilon_0 k T_e / n_e e^2\right)^{1/2}. \tag{3}$$

Here, ϵ_0 is the permittivity of free space, k is the Boltzmann constant, T_e is the electron temperature, and n_e is the electron density. For weakly degenerate plasmas, calculating the Debye length at an effective temperature will result in a smooth interpolation between the degenerate and classical plasma regimes [21, 22]. The collective scattering regime can be distinguished from the non-collective regime with the scattering parameter α

$$\alpha = \frac{1}{k\lambda_S} \tag{4}$$

where $\alpha > 1$ for collective scattering and $\alpha < 1$ for non-collective scattering. For small energy transfers, where the incident wave vector is approximately equal to the scattered wave vector $k_0 \approx k_s$ and $k_0 = 2\pi E_0/hc$, the magnitude of the scattering vector, $\mathbf{k}$, can be approximated by

$$k = |\mathbf{k}| = 2k_0 \sin(\theta/2) = 4\pi \frac{E_0}{hc} \sin(\theta/2). \tag{5}$$

This relation shows that the scattering parameter, α, is dependent on the scattering angle, θ, the energy of the probe radiation, E_0, through the scattering vector, and the plasma parameters, T_e, n_e, through the screening length. Therefore, to probe dense plasmas the choice of scattering angle and incident probe energy is critical for achieving the desired scattering regime. For example, to access collective scattering, $\alpha > 1$, in a weakly degenerate solid-density plasmas with $T_e = \epsilon_F = 15$ eV, we require forward scattering with $\theta = 40^\circ$ and x-ray energies $E_0 \leq 3$ keV. For these conditions, higher x-ray probe energies, $E_0 > 3$ keV will result in non-collective scattering.

X-ray scattering in the non-collective regime will result in an unshifted Raleigh peak and a Compton peak downshifted in energy. As derived from first principles for degenerate plasmas, the intensity of the scattered radiation is proportional to n_e and the width of the Compton downshifted peak is proportional to the square root of the Fermi electron temperature of the plasma. For a Fermi degenerate plasma the width of the downshifted peak is proportional to $n_e^{1/2}$. The Fermi-Dirac distribution function shown below [23] can be applied to Fermi degenerate or weakly degenerate plasmas, $T_e < \epsilon_F$, where $v_F = (2\epsilon_F/m_e)^{1/2}$is the Fermi velocity, β is the angle between the x-axis and the electron velocity direction v_x which is the velocity component along the scattering vector $\mathbf{x} = \mathbf{k} = \mathbf{k_{scatt}} - \mathbf{k_{incd}}$ [23], k is the magnitude of the plasma electron wave vector and m^* is the effective electron mass.

$$f_0\left(\frac{v_x}{v_F}\right) \propto \int_0^{2\pi} \frac{\left(v_x/v_F \cos\beta\right)^2 \tan\beta d\beta}{e^{\left(\left(\frac{v_x}{v_F\cos\beta}\right)^2 - \eta\right)/\left(\frac{T_e}{T_F}\right)} + 1} \tag{6}$$

The chemical potential η is the energy at which the average probability of filling a quantum state is 1/2

$$\eta = \eta_0 \left(1 - \frac{\pi^2}{12}\left(\frac{k_0 T}{\eta_0}\right)^2 + ...\right) \tag{7}$$

$$\eta_0 = \frac{\pi^2\hbar^2}{2m^*}\left(\frac{3n}{\pi}\right)^{2/3}$$

where m^* is the effective electron mass and n is the number of electrons per unit volume which can be calculated from the energy density of states $N(E)$.

$$n = 2\int_0^\infty N\left(E\right) f_o(E) dE \tag{8}$$

The factor of 2 is present to account for the fact that each state has the probability to be occupied by two electrons, with spins of $\pm 1/2$, according to the Pauli exclusion principle. Direct measurement of the shape and width of the velocity distribution in a degenerate plasma using Eqs. (6-8) will provide the Fermi temperature and therefore the density of the system. In a non-degenerate plasma, on the other hand, the velocity distribution will provide a measure of the electron temperature.

For systems of interest in high-energy density science, densities are in the range of solid density and higher. For example, probing solid-density beryllium with mass density of $\rho = 1.85$ g/cc in backscatter geometry, $\theta = 140^\circ$ and with a moderate x-ray energy source such as chlorine K$-\alpha$ at $E_0 = 2.62$ keV will access a scattering vector of $|\mathbf{k}| = 2.5\times10^{-10}$ m^{-1} (cf. Eq. (5)). In this case, the Compton feature will be shifted from E_0 by

$$\Delta E_C = \frac{\hbar^2 k^2}{2m_e} = 24\text{eV}. \tag{9}$$

The spectral shape of the Compton line is determined by Eqs. (6-8) and the width can be calculated from the Fermi velocity

$$\delta E_C = 2\frac{E_0}{c} v_F sin(\theta/2) = \hbar k v_F = 38\text{eV}. \tag{10}$$

This suggest an x-ray probe bandwidth of $\Delta E/E < 15$ eV to resolve the Compton peak, Rayleigh peak and the spectral broadening.

Experiments that apply forward scattering to measure the collective x-ray scattering spectrum impose more stringent requirements on the x-ray source than non-collective backscattering measurements described above. In forward scatter, the scattering spectrum yields the collective electron oscillation peak, i.e. plasmons up-shifted and down-shifted from the incident x-ray energy. The plasma dispersion relation providing the plasmon energy shift can be approximated by a modified Bohm-Gross relation for small values of $\mathbf{k}$, i.e. large values of α,

$$\omega_{pl}^2 = \omega_p^2 + 3k^2 v_{th}^2(1 + 0.088 n_e \Lambda_e^3) + \left(\frac{\hbar k^2}{2m_e}\right)^2 \tag{11}$$

where $v_{th} = \sqrt{k_B T/m_e}$ is the thermal velocity and $\Lambda_e = h/\sqrt{2\pi m_e k_B T}$ is the thermal wave length. In Eq. (11), the first term is a result of electron oscillations in the plasma [24], the second term represents the effect on propagation of the oscillation from thermal pressure [25]. The third term includes degeneracy effects from Fermi pressure, [26], and the last term is the quantum shift. The quantum shift combined with the electron oscillations accounts for most of the measured shift of the Compton peak in relation to the unshifted Raleigh peak. Therefore, the scattered spectrum provides a sensitive measure of the plasma electron density.

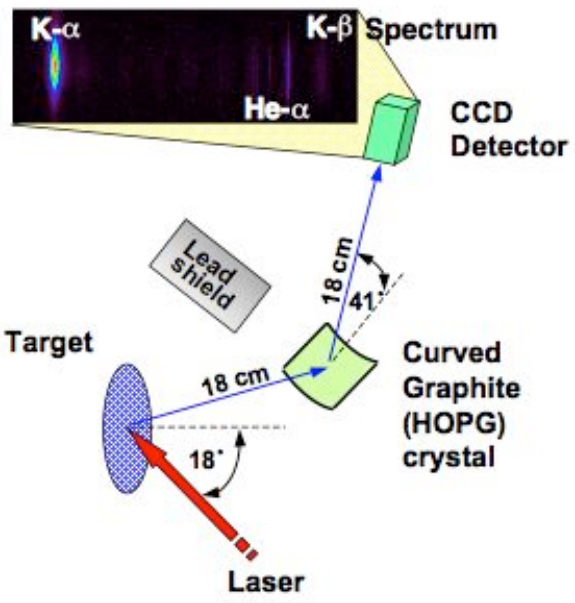

FIG. 1: Experimental setup: An isotropic K-alpha source is produced when a ultra-intense laser is incident on a thin foil. The radiation is dispersed using a high efficiency HOPG spectrometer and collected on a CCD or Image Plate.

For example, a forward scattering angle of $\theta = 40^\circ$ and Chlorine K$-\alpha$ x-ray probe at $E_0 = 2.62$ keV will access a scattering vector of $|\mathbf{k}| = 0.9\times10^{-10}$ m^{-1} (cf. Eq. (5)). Probing solid-density beryllium at $T_e = 15$ eV in this scattering geometry will measure a shifted plasmon at

$$\Delta E_{pl} = \hbar\omega_{pl} = 27\text{eV}. \tag{12}$$

In this regime, broadening of the plasmon peak by Landau damping and collisional damping [27] occurs and can be calculated with the dynamic structure factor $S(\mathbf{k},\omega)$ [28, 29] resulting in $\delta E_{pl} \approx 15$ eV. To resolve the spectral broadening of the plasmon thus requires a x-ray probe bandwidth of $\Delta E < 10$ eV.

CONVERSION EFFICIENCY MEASUREMENTS OF CHLORINE K$-\alpha$ AT 2.62 KEV

Chlorine K-α x-rays (2.62 keV), corresponding to the $1s-2p$ transition in weakly ionized Cl, were produced using two lasers, Europa and Callisto, located at the Jupiter

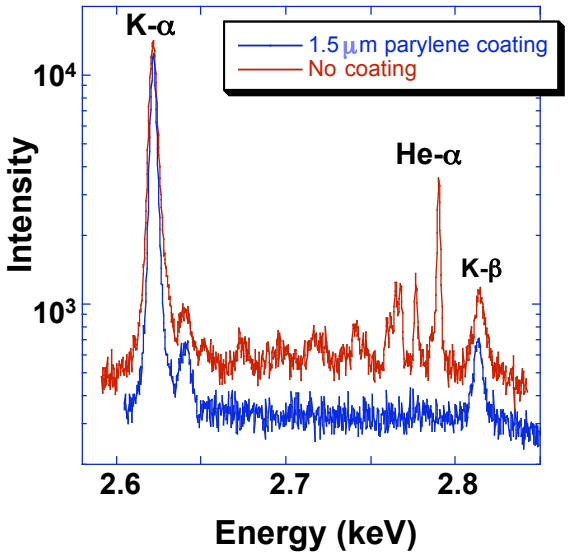

FIG. 2: K-α spectra from 12.5 μm thick Saran targets with and without coating, taken at Europa. The number of K-α photons produced does not significantly vary between the targets with and without coating.

laser facility, LLNL. Europa is a 100 fs Ti:Sapphire laser with a wavelength of 800 nm, focal spot size of ~ 28 μm, and energy ranging from roughly 100 mJ to 1.2 J. Callisto has a maximum achievable energy of 15 J and operates at 800 nm or 400 nm. The focal spot size is about 3-5 μm in diameter and the pulse duration can be varied from 100 fs to 1 ps. Cl was chosen because of its low atomic number and moderate K-α line energy. The low Z of the material will help reduce the amount of background due to Bremsstrahlung radiation, proportional Z^2, which contributes to the background level of the Cl spectrum in the energy range of interest. The energy of the Cl K-α is sufficient to penetrate plasmas of electron densities on the order of $10^{23}/cm^3$, but low enough for collective scattering in the forward direction.

Emission of K$-\alpha$ radiation resulting from target atom ionization by laser produced hot electrons was observed. A graphite (HOPG) crystal in the mosaic focusing mode [2, 5] has been applied to disperse the scattered radiation onto a charged coupled device (CCD) for laser intensities below $10^{18}W/cm^2$ and an image plate (IP) to access data at higher laser intensities, FIG.1. The HOPG crystal provides high reflectivity [4] allowing emission measurements at laser energies as low as $E_L = 60$ mJ. It can be seen from FIG.2 that the K-α bandwidth $\Delta E/E = 2 \times 10^{-3}$ is sufficient to resolve the downscattered plasmon peak. The peak signal-to-noise ratio (SNR) for the 1.5 μm coated target, about 70 for coated targets, is sufficient for adequate scattering statistics.

Various Cl containing target compositions, NaCl, KCl, and Saran $(CH\text{-}Cl\text{-}CH_2)_N$ were explored to observe the effect, if present, of free electron population and dielectric properties of the target on K-α production. Parylene-N (C_8H_8) target coating thicknesses were explored to investigate the effects of laser pre-pulse on the induced plasma. Parylene-N is a linear, highly crystalline polymer that can be formed as a continuous film coating over target materials. Since an initial laser pre-pulse may be prematurely heating the plasma, a target coating was developed to absorb the pre-pulse energy burst and allow more interactions of the main pulse with Cl atoms in the solid. The use of an overcoating eliminated a significant amount of emission from plasma "'blow-off"', FIG 2, which occurs under intense laser plasma interactions, such as Cl He-α radiation corresponding to the $1s^2\mathrm{S}{-}1s2p^1\mathrm{P}^\circ$ transition. The total number of K-α photons produced does not vary much between coated and uncoated targets, whereas contribution from blow-off emission decreases greatly with a coated target.

Conversion efficiencies ($C.E.$), assuming isotropic emission, of laser energy to K-alpha energy using a curved HOPG crystal were calculated [5] from the interpreted number of counts detected on the CCD, I, according to

$$C.E. = \frac{4\pi I q_{ccd} q_{eh} F}{T_r r_p d Q \gamma E_L} \tag{13}$$

with F being the focal distance, d the size of the crystal in the non-dispersive direction, γ the mosaic spread of the crystal, T_r the filter transmission, r_p the crystal peak reflectivity, Q the CCD quantum efficiency, and E_L the energy of the laser.

The number of counts on the ccd were determined from integration of the K-alpha peak in the sagittal and dispersive directions with background subtracted. Each count on the ccd corresponded to 3.5 electron-hole (eh) pairs, q_{ccd}, each requiring 3.6 eV to create, q_{eh}. The number of photons $N_{photons}$ corresponding to each count on the ccd

$$N_{photons} = \frac{I \times 3.5(eh/count) \times 3.6(eV/eh)}{2622(eV/photon)} \tag{14}$$

is approximately $4.8 \times 10^{-3}/count$. For typical 12.5 μm Saran targets shot with a laser intensity of $1{\times}10^{18}W/cm^2$ ($E_L \sim 1$ J) the number of photons detected was $\sim 3.2{\times}10^5$. Correcting for the solid angle of the spectrometer, the total number of photons created was $\sim 3.1{\times}10^{10}$. Conversion efficiency as a function of target foil thickness for Saran targets is shown in FIG.3(a) for front side emission and laser intensities ranging from 10^{17} to $10^{21}W/cm^2$ at best focus. The error bars represent the standard deviation in the data, which consisted of approximately 20 data points. There is no apparent dependence of conversion efficiency on target foil thickness for targets ranging from 12.5 -50 μm. Conversion efficiencies for varying Parylene-N target coating thickness

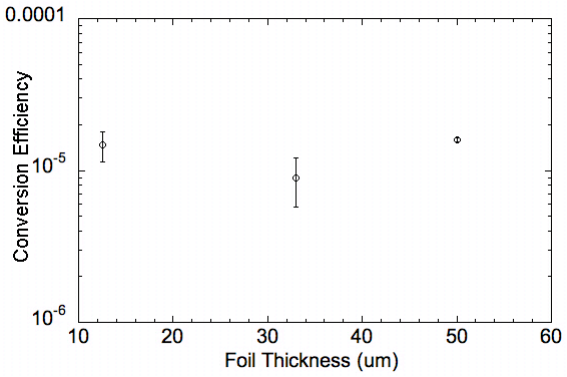

(a)

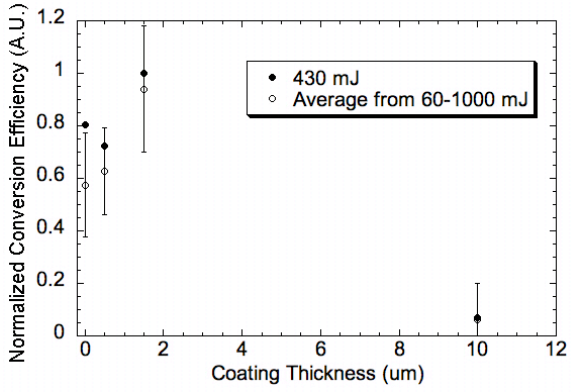

(b)

FIG. 3: a.) Conversion efficiencies for front side emission from Saran foil targets averaged over laser intensities ranging from 10^{17} to $10^{21} W/cm^2$ as a function of foil thickness. b.) Normalized conversion efficiencies of 12.5 μm thick Saran foils with varying Parylene-N target coating thicknesses, plotted for a specific laser energy and an average over all laser energies.

for 12.5 μm Saran foils are shown in FIG.3(b). There is weak dependance of $C.E.$ on coating for Parylene-N thicknesses below 2 μm. However, a significant decrease in $C.E.$ for a coating thickness of 10μm was observed. This could be due to the fact that the hot electrons must travel further into the target before they can cause K-shell ionization and roughly 13% are absorbed in the 10μm of Parylene-N as they escape the target.

Conversion efficiencies for NaCl, KCl, and Saran foils of thickness ranging from one to fifty microns were measured for laser intensities of 10^{17} to $10^{21} W/cm^2$. There was no observed dependence of C.E. on laser intensity FIG.4 for data taken using Saran targets with thicknesses above 12.5 μm. The relative error for each shot is estimated to be 10 % accounting for uncertainty in the laser

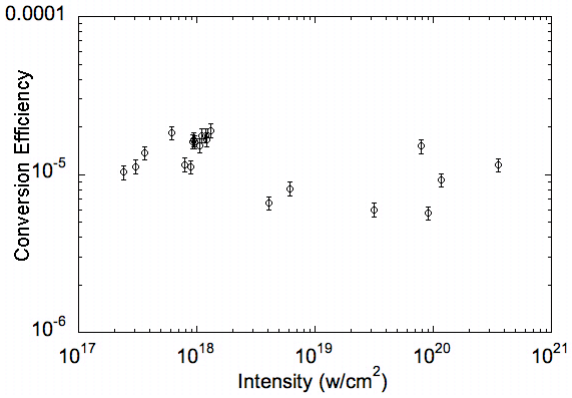

FIG. 4: Conversion efficiency vs. laser intensity at best focus for front side emission of Cl K-α X-rays from Saran foil targets. For intensities below $10^{18} W/cm^2$, data were taken at Europa, LLNL and data taken above this intensity were collected at Callisto, LLNL.

TABLE I: Conversion efficiencies for front side emission for various target thickness and Cl containing compositions for $I_{laser} \sim 10^{18} W/cm^2$.

Thickness(μm)	Saran	NaCl	KCl
$10 - 12.5$	$1.5x10^{-5}$	$1.3x10^{-5}$	$1.4x10^{-5}$
$5 - 5.5$	$- - -$	$8.1x10^{-6}$	$9.2x10^{-6}$
1	$- - -$	$6.1x10^{-6}$	$5.0x10^{-6}$

energy (50 mJ), noise in the spectra ($\sim$ 1 %), and CCD quantum efficiency (cf. Eq. (13)).

A slight increase with increasing laser intensity was observed for target thicknesses $<$ 12.5 μm, TABLE 1. For the thinner foils, such as 1 μm thick KCl, conversion efficiencies either remained constant or decreased slightly 5-10% with increasing laser intensity. All target compositions displayed comparable conversion efficiencies. For NaCl and KCL, $C.E.$ decreased with decreasing target thickness, which was probably a result of the targets being destroyed by the pre-pulse before a significant amount of x-rays could be produced.

K$-\alpha$ SCATTERING SPECTRA FROM FUSION PLASMAS

Characterizing inertial confinement fusion capsule implosion conditions will be one of the most challenging application of spectrally-resolved x-ray scattering. The capsules will be heated and compressed by four successive shocks that are driven by soft x-rays created in laser-heated high$-Z$ hohlraums. Temporally and spectrally resolved x-ray scattering experiments from fusion capsule implosions may provide a means for directly measuring the capsule fuel density and provide information

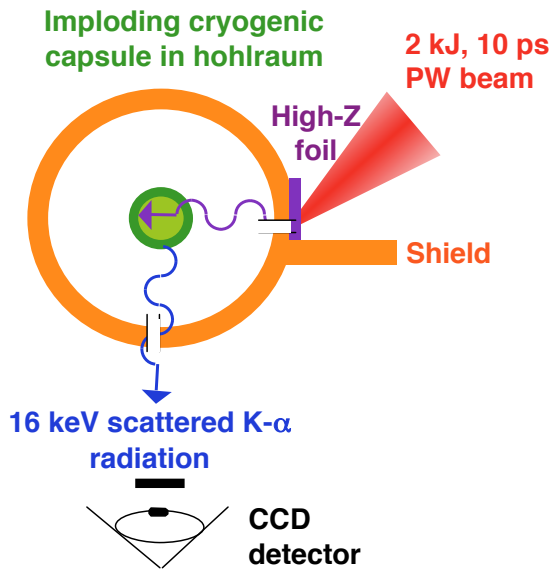

FIG. 5: A schematic of an x-ray scattering experiment on a hohlraum-driven fusion capsule implosion is shown.

on shock timing and ablator density. This experiment may be achieved by producing an energetic K$-\alpha$ source in close proximity of the implosion and by observing the scattered radiation through collimators that will restrict the detector to view the central 0.6 mm diameter region of the implosion.

Figure (5) shows a schematic of an x-ray scattering experiment on a hohlraum driven implosion, For this example, Zr K$-\alpha$ radiation at $E_0 = 15.7$ keV is considered, This probe energy is required to penetrate through the fuel and to probe the implosion shortly before formation of the hot spot. Lower energy probe radiation may be used early in the implosion when the fuel density is below 10^{24}cm^{-3}. The K$-\alpha$ radiation may be produced with a kilo-joule short-pulse laser such as the Advanced Radiographic Capability presently being planned for the NIF to produce $> 10^{12}$ photons in the K$-\alpha$ line. This expected photon number, the K$-\alpha$ bandwidth, and the expected temporal resolution of ~ 10 ps will be sufficient to provide a snap-shot measurement of the capsule conditions during the implosion.

Data at various times during the implosion may be obtained by varying the delay of the short-pulse laser with respect to the implosion. We find that the spectral width of the scattering spectra changes by as much as $\Delta E/E =$ 20 % when probing the implosion at (15.8 ± 0.1) ns just (0.6 ± 0.1) ns before peak density. This width is readily measurable. The spectral shape of the scattering data will measure the capsule adiabat, T_e/T_F, and n_e. In addition, an absolutely calibrated detector will provide independent information on the electron density from the absolute intensity of the scattering signal. Thus x-ray scattering will measure the compression of the fuel to high density which is important for ICF.

Figure (6)shows calculated Zr K$-\alpha$ scattering spectra for typical fusion capsule conditions near the rise of the fourth shock (15.8 ns in this example). These calculations use the full theoretical form factor in the random phase approximation [22**?**] and apply calculated densities and temperatures from the radiation-hydrodynamic code HYDRA [30]. A shell model was used to calculate the scattering spectra for the conditions $r_i < S(n_e, T_e, Z, \omega) < r_k$ and weigh the contribution from each shell according to the number of scattering electrons in the shell, $g_k = n_e(r_k^3 - r_i^3)$, $r_k, r_i \leq 0.3$ mm.

First, we have calculated the scattering spectra for implosions where the timing of the last shock has been varied by ± 100 ps by properly advancing or delaying the rise of the laser pulse, Fig. (6(a)). The scattering from a properly timed shock ($\tau = 0$) shows a parabolic intensity distribution indicating a Fermi degenerate fuel with an electron density of $5 \times 10^{24}\text{cm}^{-3}$. The main scattering feature is Compton down-shifted in energy by $\Delta E \simeq 0.5$ keV from the incident energy E_0, where a small Rayleigh peak is observed from elastic scattering off bound electrons in beryllium. At this time only a very small amount of Be is present in the scattering volume and the scattering spectrum provides accurate data on the fuel density.

If the fourth shock arrives 100 ps earlier ($\tau = -100$ ps) the fuel will be more compressed than in the case of $\tau = 0$. The additional broadening of the scattering spectra is a measure of the increased density, $n_e = 9 \times 10^{24}\text{cm}^{-3}$. In addition, the scattering spectrum is slightly more red-shifted and not parabolic showing low intensity wings at higher energy. These features indicate the heating of the fuel and the beginning of the hot spot formation. The Rayleigh scattering feature at E_0 shows a large signal because cold Be fuel blow off gets into the scattering volume when the capsule implosion is at smaller radii.

If the fourth shock arrives 100 ps later ($\tau = 100$ ps) the fuel in the scattering volume will be significantly less dense than for the case of $\tau = 0$ and the scattering spectra are rather narrow. Moreover, the low-density hot core of the implosion is contributing to the scattering spectra resulting in a non-parabolic scattering spectrum. No Rayleigh scattering feature can be observed at E_0 since no Be ablator blow off transverses the scattering volume when the capsule implosion is at larger radii.

This analysis shows that a properly timed K$-\alpha$ scattering experiment can measure the Fermi-degenerate fuel in a ICF implosion when restricting the scattering volume with collimating shields. Figure (6(b) indicates that the spectral width and intensity of the Compton scattering feature accurately measure the fuel electron density. The calculations indicate the expected dependency on $v_F \sim \sqrt(T_F)$ (Eq. (10)) and n_e, respectively. Figure (6(c) shows the dependency of the spectral shape

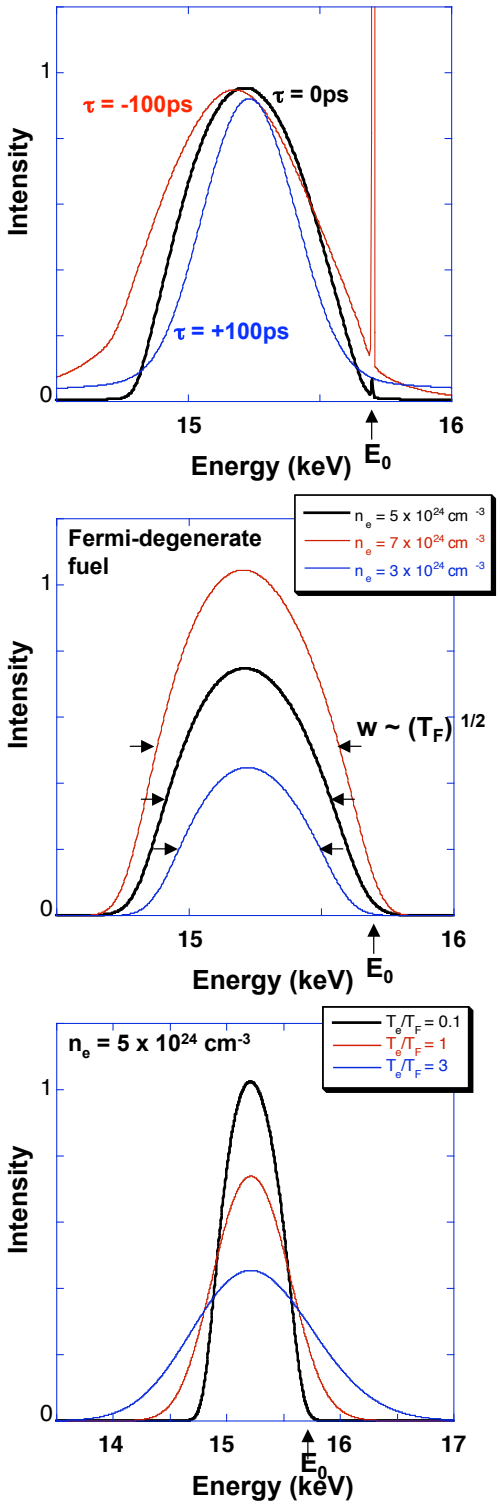

FIG. 6: Synthetic x-ray scattering spectra in arbitrary but linear units calculated for inertial confinement fusion capsule conditions. (a) Scattering spectra at the rise of the fourth shock with the field of view restricted to $r \leq 0.3$ mm. Scattering spectra are normalized to peak intensity of the Compton down-shifted line to indicate sensitivity of the spectral shape to ICF capsule conditions. (b) Sensitivity of the scattering spectra to fuel electron density. (c) Sensitivity of the scattering spectra to fuel temperature.

on the electron temperature to Fermi temperature ratio. With increasing T_e we find that the scattering spectrum transitions from a parabolic to a Gaussian shape reflecting the transition from a Fermi to a Boltzmann electron velocity distribution function. Thus, this measurement will allow determining the fuel adiabate.

CONCLUSIONS

In summary, we have developed K$-\alpha$ x-ray sources for x-ray scattering measurements to characterize plasma conditions and the optical properties in dense matter. We find that the spectral properties are well suited for non-collective as well collective scattering application. The conversion efficiency, on the other hand, is 2 order of magnitude smaller than for ns-laser produced K-shell sources, Additional work is required to optimize K$-\alpha$ sources, e.g. by applying grating and rough-surface targets [31, 32] to attempt scattering from radiatively heated or shock compressed material in the near future.

ACKNOWLEDGMENTS

This work was performed under the auspices of the U.S. Department of Energy by the University of California Lawrence Livermore National Laboratory under contract number No. W-7405-ENG-48. This work was also supported by the Laboratory Directorate Research and Development grant No. 05-ERI-003, the Lawrence Livermore National Laboratory Student Employment Graduate Fellowship program, and the Alexander-von-Humboldt foundation.

[1] S. H. Glenzer *et al.*, Phys. Rev. Lett. *submitted* (2006).
[2] S. H. Glenzer *et al.*, Phys. Rev. Lett. **90**, 175002 (2003), *ibid* Phys. Plasmas **10**, 2433 (2003).
[3] G. Gregori *et al.*, Phys. Plasmas **11**, 2754 (2004). *ibid*, J. Quant. Spectrosc. Radiat. Transfer, **99**, 225 (2006).
[4] F. J. Marshall and J. A. Oertel, Rev. Sci. Instrum. **68**, 735 (1997).
[5] A. Pak *et al.*, Rev. Sci. Instrum. **75**, 10 (2004).
[6] S. Tzortzakis, P. Audebert, P. Renaudin, et al. J. Quan. Spectr. Trans. **99**, 614 (2006).
[7] D. Riley *et al.*, Phys. Rev. Lett. **84**, 1704 (2000).
[8] H. S. Park *et al.*, Phys. Plasmas **13**, 056309 (2006).
[9] F. Y. Khattak *et al.*, Phys. Rev. E **74**, 027401 (2006).
[10] M.K. Urry *et al.*, J. Quan. Spectr. Trans. **99**, 636 (2006).
[11] A. Höll *et al.*, High Energy Density Science *submitted*
[12] V. Ayvazyan, *et al.*, Eur. Phys. J. D, **37**, 297 (2006).
[13] J. Feldhaus, J. Arthur, J. B. Hastings, J. Phs. B **38**, S799 (2005).
[14] R. W. Lee *et al.* J. Opt. Soc. Am. B **20**, 770 (2003).
[15] O. Guilbaud *et al.*, Eur. Phys. J. D, **40**, 125 (2006).
[16] H. A. Baldis *et al.*, Rev. Sci. Instrum. **73**, 4224 (2002).

[17] P. Beiersdorfer, R. Shepherd, R. C. Mancini, H. Chen, J. Dunn, R. Keenan, J. Kuba, P. K. Patel, Y. Ping, D. F. Price, and K. Widmann, *in* Proceedings of the 4th US-Japan Workshop on Plasma Polarization Spectroscopy, Kyoto, Japan, February 4-6, 20041, T. Fujimoto and P. Beiersdorfer, editors, NIFS Proceedings Series No. NIFS-PROC-57 (National Institute for Fusion Studies, Toki, Japan 2004), p. 40-46.
[18] C. P. J. Barty et. al., Nucl. Fusion **44**, S266 (2004). J. D. Zuegel et. al., Fusion Science and Tech. **49** 453-482 (2006).
[19] E. I. Moses et al., Fusion Sci. Tech. **47**, 314 (2005).
[20] P. Neumayer, G. Gregori, A. Ravasio, M. Koenig, D. Price, K. Widmann, M. Bastea, O. L. Landen, and S. H. Glenzer, Rev. Sci. Instrum. **77**, 317 (2006).
[21] J. F. Perrot and M.W.C. Dharma-wardana, Phys. Rev. B **62**, 16536 (2000).
[22] G. Gregori *et al.*, Phys. Rev. E **67**, 026412 (2003).
[23] O. L. Landen *et al.*, J. Quant. Spectrosc. Radiat. Transfer, **71**, 465 (2001).
[24] L. Tonks and I. Langmuir, Phys. Rev. **33**, 195 (1929).
[25] D. Bohm and E. P. Gross, Phys. Rev. **75**, 1851 (1949).
[26] R. Zimmerman, *Many-Particle Theory of Highly Excited Semiconductors* (Teubner, Leipzig, 1987).
[27] H. Reinholz *et al.*, Phys. Rev. E **62**, 5648 (2000).
[28] A. Höll *et al.*, Eur. Phys. J. D **29** 159 (2004).
[29] R. Redmer *et al.*, IEEE Trans. Plasma Science **33** , 77 (2005).
[30] M. M. Marinak, G. D. Kerbel, N. A. Gentile, O. Jones, D. Munro, S. Pollaine, T. R. Dittrich, and S. W. Haan, Physics of Plasmas 8, 2275 (2001).
[31] M. M. Murnane *et al.*, Appl. Phys. Lett. **62**, 1068 (1993).
[32] G. Kulcsar *et al.*, Phys. Rev. Lett. **82**, 5149 (2000).